J. Phys. B: At. Mol. Opt. Phys. **23** (1990) 4549–4572. Printed in the UK

The multichannel eikonal theory of electron–hydrogen collisions: I. Excitation of H(1s)

E J Mansky and M R Flannery

School of Physics, Georgia Institute of Technology, Atlanta, Georgia 30332-0430, USA

Received 15 May 1990

Abstract. The integral and differential cross sections for the electronic excitation of the $2l$ and $3l$ states of hydrogen obtained by the multichannel eikonal theory in a 10-channel basis are reported. The λ, R and I parameters for the 2p state of hydrogen at 54.40 and 350 eV are also provided. Good agreement with the experimental data of Mahan *et al* for the integral cross sections $\sigma_{1s\rightarrow 3l}$ is achieved by the present updated and extended multichannel eikonal theory. Two general conclusions follow from the results reported in this paper: (a) the first Born results underestimate experiment in s $\rightarrow$d transitions and (b) indirect coupling mechanisms for the excitation of the 3d state of hydrogen are important and cannot be neglected. These conclusions indicate that the pseudostate basis used in a number of optical potential model calculations needs further refinement in the intermediate energy region.

1. Introduction

The integral cross sections for the electron impact excitation of atoms initially in an excited state are of fundamental importance in the modelling of laboratory and astrophysical plasmas. Although a great deal of theoretical effort has been devoted to computing excitation cross sections $\sigma_{n,n'}(n, n' \geq 1)$ for hydrogen and helium, basic theoretical problems still remain after nearly thirty years of work. Within the last decade experiments on low-temperature plasmas (Burgess *et al* 1978, 1980) have shown that either widely used semi-empirical cross sections (Johnson 1972) are in error by a factor of five or more; or highly non-Maxwellian electron velocity distributions are required to explain the laser-excited fluorescent decay of these hydrogen plasmas (T_e = 0.4–0.8 eV). Also, within the last five years, the first direct experimental measurement of inelastic differential cross sections (from the 2^3S state of He to the 2^3P, 3^3S, 3^3P, 3^3D and $n = 4$ states of helium) has been made (Müller-Fiedler *et al* 1984). These experimental results, together with the basic theoretical problem of providing accurate, converged results for the $\sigma_{2,3}$ cross sections in hydrogen and helium are the primary motivations of the present work.

The multichannel eikonal theory of electron–atom collisions was originally developed by Flannery and McCann (1974a, b, c, 1975a) for $e^- + A^*$ collision processes. At that time only electron impact excitation of He($2^{1,3}$S) was considered due to computational limitations. In the second paper of this series the original results of the multichannel eikonal theory (MET) of Flannery and McCann (1975a) are updated and extended to the excitation of hydrogen initially in the 2s and 2p states. In this paper

0953-4075/90/244549+24$03.50

(paper I) the excitation of H(1s) to the $2l$ and $3l$ states of H is considered, in order to provide a better assessment of the accuracy of the MET inelastic integral cross section results, due to the greater availability of measurements and other theoretical treatments in the case of the excitation of ground state targets. The overall goal of this series of papers (and a corresponding pair of papers for helium) is the elucidation of the excitation cross sections $\sigma_{n,n'}(n, n' = 2, 3)$ for $e^- + H^*$, He^* collisions. The systematic trends observed in the MET results can then be compared with the semi-empirical cross sections (Johnson 1972, Vriens and Smeets 1980) currently used to model laboratory and astrophysical plasmas.

In this paper the present semiclassical MET results are compared with a number of other theoretical results including the distorted-wave second Born approximation results of Kingston and Walters (1980) and a number of close-coupling results. Principal among the latter theories are the 3-state close-coupling results of Kingston *et al* (1976), the 6-state coupled channels optical model results of McCarthy and Stelbovics (1983), the 18-state optical model results of Callaway *et al* (1987) and the multipseudostate results of van Wyngaarden and Walters (1986b). While the eikonal approximation is a high-energy, small-angle approximation, the use of the semiclassical coordinate representation in the MET allows for the implicit inclusion, via the impact parameter ρ, of the infinite number of partial waves important at high impact energies in general (section 3) and in electron–excited atom collisions in particular (paper II). At lower energies comparison of the MET with the exact close-coupling theories previously mentioned will be important in determining the range of validity of the eikonal approximation. In particular comparison of the MET results with exact close-coupling theories with comparable basis sets (e.g. the results of Callaway (1985) and McCarthy and Stelbovics (1983)) will provide a detailed test of the semiclassical eikonal approximation used in this paper (see tables 2 and 3 in section 3).

A short summary of the original MET of Flannery and McCann is provided in section 2, while a complete discussion and comparison of the current MET results, for the integral and differential cross sections, with available experimental and theoretical data are given in section 3. The conclusions of the paper are given in section 4. Atomic units are used throughout.

2. Theory

Since the MET of $e^- + A^*$ collision processes has already been discussed in detail by Flannery and McCann (1974a–d, 1975a, b) in a series of papers, only a basic summary is needed. This paper treats the collision process,

$$e^- + H(1s) \rightarrow e^- + H(1s, 2s, 2p_0, 2p_{\pm 1}, 3s, 3p_0, 3p_{\pm 1}, 3d_0, 3d_{\pm 1}, 3d_{\pm 2})$$

where the hydrogen atom is initially in the 1s ground state, and a 10-channel basis will be used to represent the target H. In contrast to earlier MET results for H (Flannery and McCann 1974c), no pseudostates are used in the present basis set. The MET scattering amplitude for excitation of the target H from the initial state i to any of the states in the basis set (denoted by n) is given by

$$f_{ni}(\theta) = -(\mathrm{i})^{\Delta+1} \int_0^\infty J_\Delta(q'\rho)\{I_1(\rho, \gamma(\theta)) - \mathrm{i}I_2(\rho, \gamma(\theta))\}\rho \, \mathrm{d}\rho \qquad (1)$$

where θ is the electron scattering angle. The integrals I_1 and I_2 are defined as

$$I_1(\rho,\gamma(\theta)) = \int_{-\infty}^{\infty} \mathrm{d}z\, \kappa_n(\rho,z) \frac{\partial C_n(\rho,z)}{\partial z} \exp(\mathrm{i}\gamma(\theta)z) \tag{2a}$$

$$I_2(\rho,\gamma(\theta)) = \int_{-\infty}^{\infty} \mathrm{d}z \left(\kappa_n(\rho,z)(\kappa_n(\rho,z) - k_n) + \frac{\mu}{\hbar^2} V_{nn} \right) C_n(\rho,z) \exp(\mathrm{i}\gamma(\theta)z) \tag{2b}$$

where the amplitude functions $C_n(\rho,z)$ are the solutions of the following first-order partial differential equations,

$$\mathrm{i}\frac{\hbar^2}{\mu}\kappa_n(\rho,z)\frac{\partial C_n(\rho,z)}{\partial z} + \left\{ \frac{\hbar^2}{\mu}\kappa_n(\rho,z)(\kappa_n(\rho,z) - k_n) + V_{nn}(\rho,z) \right\} C_n(\rho,z)$$
$$= \sum_{j=1}^{N} V_{nj}(\rho,z) C_j(\rho,z) \exp\{\mathrm{i}(k_j - k_n)z\} \tag{3}$$

which is solved for the N states in the basis set subject to the asymptotic boundary condition $C_n(\rho, z \to -\infty) = \delta_{ni}$. In the MET, a semiclassical, impact parameter representation is used for the wavefunction for the system composed of e^- + target atom. This results in picturing the scattering event as an interaction of an e^-, with impact parameter ρ and distance along the trajectory z, with the target H initially in the ground state. As the projectile e^- proceeds along its trajectory, with impact parameter ρ, a large number of channels in the target H are populated, with probability $|C_n(\rho,z)|^2$. The complex amplitudes $C_n(\rho,z)$ associated with these probabilities are propagated within each channel n with a local wavenumber κ_n;

$$\kappa_n = \kappa_n(\rho,z) = \left(k_n^2 - \frac{2\mu}{\hbar^2} V_{nn} \right)^{1/2}$$

where k_n is the asymptotic wavenumber associated with channel n. The remaining parameters in equations (1) and (2) are: J_Δ is an ordinary Bessel function of the first kind and integer order $\Delta = m_i - m_n$, the difference of the magnetic quantum numbers of channels i and n; and $q' = k_n \sin\theta$, $\gamma(\theta) = k_n(1 - \cos\theta)$.

The electrostatic matrix elements V_{nj} appearing in equation (3) are defined as follows

$$V_{nj}(\boldsymbol{R}) = \langle \varphi_n \mid V(\boldsymbol{r},\boldsymbol{R}) \mid \varphi_j \rangle \equiv V_{nj}(R,\Theta)\exp(\mathrm{i}\Delta\Phi)$$

with the atomic states given by the electronic wavefunctions $\varphi_n(\boldsymbol{r})$. The differential and integral cross sections are then given by

$$\frac{\mathrm{d}\sigma_{ni}(\theta)}{\mathrm{d}\Omega} = \frac{k_n}{k_i} |f_{ni}(\theta)|^2 \tag{4a}$$

$$\sigma_{ni} = \int \frac{\mathrm{d}\sigma_{ni}(\theta)}{\mathrm{d}\Omega} \mathrm{d}\Omega = 2\pi \int_0^\pi \frac{k_n}{k_i} |f_{ni}(\theta)|^2 \sin(\theta) \mathrm{d}\theta. \tag{4b}$$

Here we are concerned with the scattering of e^- in the intermediate to high energy region (i.e. from 14 to 1000 eV) where all N channels in the basis set are open. Two

key assumptions are made in the MET results reported here. First, the influence of electron exchange is omitted completely. Secondly, straight-line trajectories are assumed for the e^-. Clearly the first assumption will greatly affect the results for elastic scattering, and inelastic differential cross sections at large scattering angles ($\theta \geq 50°$). However, since our primary goal is the accurate prediction of *integral* cross sections $\sigma_{i,n}$, we only need accurate inelastic differential cross sections in the forward direction ($0° \leq \theta \leq 40°$). In $e^- + A^*$ collision processes, the assumption of straight-line trajectories for the e^- should be accurate since the large induced polarization causes scattering mainly in the forward direction which is well described by the diffractive-like Bessel function J_Δ in equation (1). The assumption of straight-line trajectories may, however, be removed and account taken of the curvature of the projectile's trajectory for large scattering angles. The modifications required to account for the curvature of the trajectory within the MET have been done by McCann and Flannery (1975, 1978) in the context of rotational excitation in atom (ion)–molecule scattering.

The central difficulty in computing excitation cross sections between excited states of atoms is taking into account the influence that the strong multipole moments induced in the target atom have on the scattering amplitude. These multipole moments, coupling the excited states together, can exceed by a factor of ten or more those coupling the ground state to the rest of the basis set. Hence neglect of distant trajectories, with impact parameters $\rho \geq 250\ a_0$, in the computation of the $\sigma_{2,3}$ cross section will therefore result in significant error. This is the so-called *large-ρ problem* which is the semiclassical analogue of the *large-l problem* encountered in close-coupling calculations (Callaway and McDowell 1983, Callaway *et al* 1987, Whelan and Piraux 1987, Whelan *et al* 1987).

In practice, the coupled equations (3) are solved numerically over a finite grid given by $-z_{\max} \leq z \leq z_{\max}$, $0 \leq \rho \leq \rho_{\max}$. A detailed discussion of the numerical solution of (3) and the subsequent evaluation of the integrals in (1) and (2) will be given separately (Mansky 1990a). What we are concerned with here is analytically solving the coupled equations (3) in the limit $\rho_{\max} \to \infty$ in order to include trajectories with impact parameters in the range $\rho_{\max} \leq \rho \leq \infty$. In this paper $\rho_{\max}$ will be in the range of 20–60 a_0 for the excitation of H(1s), while for H^* $\rho_{\max} \geq 200\ a_0$. In this limit only matrix elements V_{nj} in the coupled equations (3) involved in *dipole* transitions will be important, all other shorter-range terms will be negligible. This will leave, for a given N state basis set, say M different dipole-coupled transitions to consider. At this point, in order to make the resultant equations analytically tractable, one must assume that the M dipole-coupled transitions can be treated independently. That is, one must assume that terms which couple the different intermediate dipole transitions together (e.g. $V_{2p_m \to 3p_m}$) are much smaller than the terms which couple the initial state to each of the remaining M dipole channels (e.g. $V_{1s \to 2p_m}$ and $V_{1s \to 3p_m}$). This in fact will be the case in this paper for trajectories with $\rho_{\max} \leq \rho \leq \infty$. Hence the coupled equations (3) reduce, in the range $\rho_{\max} \leq \rho \leq \infty$, to a set of M independent 2-state problems,

$$i\frac{\partial C_n(\rho, z)}{\partial z} = \frac{\mu}{\hbar^2 k_n} V_{ni}^{(\text{dipole})}(\rho, z) C_i(\rho, z) e^{-i\alpha z} \tag{5}$$

where $\alpha = 2\mu(\epsilon_n - \epsilon_i)/\hbar^2(k_i + k_n)$, and $\epsilon_{i(n)}$= energy of the target H in channel $i(n)$.

The dipole interaction term, V_{ni}^{dipole} is given by

$$V_{ni}^{(\text{dipole})}(\rho,z)=\frac{d'_{ni}}{(\rho^2+z^2)}\begin{cases}\cos\Theta & \text{if } \Delta=0\\ \sin\Theta & \text{if } \Delta=1.\end{cases} \tag{6}$$

where $d'_{ni}=\sqrt{(\frac{3}{4}\pi)}d_{ni}$, with d_{ni} = dipole moment for the transition $i\rightarrow n$. Equation (5) follows directly from (3) in the large ρ limit and the fact that $\kappa_n\rightarrow k_n$ since $V_{nn}\ll\hbar^2k_n^2/2\mu$ in the range $\rho_{\max}\leq\rho\leq\infty$. Examination of the full numerical solution of the coupled equations (3) (Mansky 1990a) shows that the amplitude functions for the ground state, $C_i(\rho,z)$, is very well approximated by its initial value, $C_i=\delta_{ni}$, in the large ρ limit. This then allows (5) to be integrated, yielding an expression for the C_n in terms of modified Bessel functions $K_\Delta(\alpha\rho)$. Explicit acknowledgment of the contribution that distant trajectories make to the scattering amplitude is then made by rewriting (1) as

$$f_{ni}(\theta)=\Gamma\int_0^{\rho_{\max}}J_\Delta(q'\rho)\{I_1(\rho,\gamma(\theta))-\mathrm{i}I_2(\rho,\gamma(\theta))\}\rho\,\mathrm{d}\rho$$
$$+\Gamma\int_{\rho_{\max}}^{\infty}J_\Delta(q'\rho)I_1^{(\text{dipole})}(\rho,\gamma(\theta))\rho\,\mathrm{d}\rho \tag{7}$$

where the first term is just the original MET result, and the second represents the contribution from distant trajectories ($I_2\rightarrow 0$ in the large ρ limit). In equation (7) $I_1^{(\text{dipole})}(\rho,\gamma)$ is the large ρ limit of $I_1(\rho,\gamma)$ and is given by

$$I_1^{(\text{dipole})}(\rho,\gamma(\theta))=\int_{-\infty}^{\infty}\mathrm{d}z\left\{-i\frac{\mu}{\hbar^2k_n}V_{ni}^{(\text{dipole})}(\rho,z)\mathrm{e}^{-\mathrm{i}\alpha z}\right\}k_n\mathrm{e}^{\mathrm{i}\gamma(\theta)z} \tag{8}$$

while Γ, the outside complex phase factor, is defined: $\Gamma=-(\mathrm{i})^{\Delta+1}$. Using (6), the z integration in equation (7) can be done immediately. Then, using the identity (Gradshteyn and Ryzhik 1965)

$$\int_y^{\infty}J_n(ax)K_n(bx)x\,\mathrm{d}x=\int_0^{\infty}J_n(ax)K_n(bx)x\,\mathrm{d}x-\int_0^{y}J_n(ax)K_n(bx)x\,\mathrm{d}x$$
$$=\frac{-1}{a^2+b^2}\{ayJ_{n+1}(ay)K_n(by)-byJ_n(ay)K_{n+1}(by)\}$$

the second term in (7) is evaluated as

$$f_{ni}^{(\text{dipole})}(\theta)=\Gamma\cdot(\mathrm{i})^{\Delta}\frac{2\mu d'_{ni}}{\hbar^2}\frac{\alpha'}{q'^2+\alpha'^2}\{\chi_1J_{\Delta+1}(\chi_1)K_\Delta(\chi_2)-\chi_2J_\Delta(\chi_1)K_{\Delta+1}(\chi_2)\} \tag{9}$$

where $\alpha'=\gamma(\theta)-\alpha$. The arguments in the Bessel functions in (9) are defined as $\chi_1=q'\rho_{\max}$ and $\chi_2=\alpha'\rho_{\max}$. Equation (9) represents the present correction to the scattering amplitude, for channel basis states n dipole-coupled to the initial state. In this paper, the correction (9) is applied only to the scattering amplitudes for the transitions $1s\rightarrow 2p_m$ and $1s\rightarrow 3p_m$. Therefore, the modification to the original MET required by the large ρ problem associated with distant trajectories is summarized as

$$f_{ni}^{(\text{DMET})}(\theta)=\Gamma\int_0^{\rho_{\max}}J_\Delta(q'\rho)\{I_1(\rho,\gamma(\theta))-\mathrm{i}I_2(\rho,\gamma(\theta))\}\rho\,\mathrm{d}\rho+f_{ni}^{(\text{dipole})}(\theta)$$
$$=f_{ni}^{(\text{MET})}(\theta)+f_{ni}^{(\text{dipole})}(\theta)\qquad\Delta l=\pm1 \tag{10a}$$
$$=f_{ni}^{(\text{MET})}(\theta)\qquad\Delta l=0. \tag{10b}$$

Hereafter the present results will be denoted by DMET with the understanding that the dipole correction (9) is only used for the $1s \rightarrow 2p_m$ and $1s \rightarrow 3p_m$ transitions. That is, the dipole correction (9) is only valid for non-degenerate transitions. For the DMET calculations reported in this paper, the dipole correction (9) for dipole transitions $n \rightarrow f$ involving intermediate states $n(n > i)$ is not applied due to the much greater importance of the degenerate dipole transitions $ns \rightarrow np_m$ on the cross sections $\sigma_{1s\rightarrow 2p}$ and $\sigma_{1s\rightarrow 3p}$. The degenerate dipole transitions are included in this paper only via their inclusion in the coupled equations (3).

3. Results and discussion

3.1. Integral cross sections

The DMET results for the integral cross sections for the excitation of the 1s state of hydrogen are shown in figure 1 and displayed in table 1. In all cases the DMET results converge at high energies to the Born results (the DMET results for the $1s \rightarrow 2p, 3p$ differ from the corresponding Born results by $\leq 3\%$ for energies $E \geq 500$ eV). The improved convergence of the present DMET results at high energies, compared with the original MET results of Flannery and McCann (1974a–c), is a direct reflection of the improved numerical solution of (3) in the present calculation. Note that the choice of incident energies used in table 1 was dictated by the rapid behaviour of the inelastic integral cross sections $\sigma_{1s\rightarrow 3l}$ for the excitation of the $3l$ states of H in the intermediate energy region ($E \leq 50$ eV).

In figure 1(a) the DMET results for the integral cross section for elastic scattering are shown. As expected, the DMET results are in agreement with the experimental elastic differential cross sections of Williams (1975), as integrated by de Heer *et al* (1977), only for energies $E \geq 200$ eV. The underestimation of the DMET results at lower energies is a direct reflection of the omission of polarization distortion and electron exchange in the present calculation. When these effects are included in, for example, a distorted-wave second-order Born approximation calculation (Kingston and Walters 1980), much better agreement with experiment is obtained.

The inclusion of all couplings between the $n = 2$ and $n = 3$ states of H leads to a significant lowering of the cross sections as one can see by comparing the DMET results with the 3-state (1s–2s–2p) close-coupling results of Kingston *et al* (1976) in figures 1(b) and (c). In the case of $\sigma_{1s\rightarrow 2s}$, the DMET results are in quantitative agreement with the experimental data of Kauppila *et al* (1970), as recommended by Callaway and McDowell (1983), only for energies $E \geq 100$ eV. At lower energies the influence of electron exchange is important. This is clearly illustrated by the optical potential results of Callaway *et al* (1987) which acknowledge the couplings between the $n = 2$ and $n = 3$ states via a local optical potential with a pseudostate basis (Callaway and Oza 1985), and include electron exchange effects as well. This leads to a significant improvement in the case of the $1s \rightarrow 2s$ transition. However, in the case of the $1s \rightarrow 2p$ dipole transition, the DMET results are in good agreement with the experimental data of Long *et al* (1968) as renormalized by Bransden and McDowell (1978) for $E \geq 30$ eV, while the results of Callaway *et al* fall below experiment in the intermediate energy region (20 eV $\leq E \leq$ 54.40 eV). At much lower energies near threshold, earlier calculations of Callaway (1982), using a similar pseudostate basis set, obtained excellent agreement with the experiment of Williams (1976). These earlier results are not shown in figure 1(c) for clarity, but the energy range of interest in those works is indicated by

Table 1. DMET integral cross sections $\sigma_{1s\to nl}$ (πa_0^2).

	nl					
E (eV)	1s	2s	2p	3s	3p	3d
14	1.31	1.01, −1[a]	4.79, −1	1.18, −2	3.14, −2	1.97, −2
15	1.22	1.12, −1	5.43, −1	1.16, −2	4.95, −2	2.37, −2
16	1.15	1.18, −1	5.76, −1	1.16, −2	6.61, −2	2.56, −2
17	1.09	1.23, −1	6.24, −1	1.18, −2	8.04, −2	2.69, −2
18	1.03	1.26, −1	6.70, −1	1.21, −2	9.06, −2	2.76, −2
19	9.85, −1	1.27, −1	6.94, −1	1.26, −2	1.00, −1	2.79, −2
20	9.42, −1	1.28, −1	7.22, −1	1.30, −2	1.10, −1	2.79, −2
21	9.03, −1	1.28, −1	7.56, −1	1.34, −2	1.14, −1	2.79, −2
22	8.69, −1	1.28, −1	7.84, −1	1.37, −2	1.20, −1	2.77, −2
23	8.36, −1	1.27, −1	8.00, −1	1.40, −2	1.26, −1	2.73, −2
24	8.07, −1	1.26, −1	8.19, −1	1.42, −2	1.31, −1	2.67, −2
25	7.80, −1	1.25, −1	8.25, −1	1.44, −2	1.33, −1	2.62, −2
30	6.71, −1	1.17, −1	8.79, −1	1.48, −2	1.44, −1	2.37, −2
35	5.91, −1	1.09, −1	8.89, −1	1.46, −2	1.47, −1	2.13, −2
40	5.30, −1	1.01, −1	8.95, −1	1.42, −2	1.49, −1	1.93, −2
50	4.40, −1	8.76, −2	8.57, −1	1.31, −2	1.45, −1	1.60, −2
54.40	4.11, −1	8.27, −2	8.45, −1	1.26, −2	1.42, −1	1.49, −2
60	3.78, −1	7.71, −2	8.25, −1	1.20, −2	1.38, −1	1.38, −2
70	3.32, −1	6.86, −2	7.75, −1	1.10, −2	1.31, −1	1.21, −2
80	2.97, −1	6.18, −2	7.34, −1	1.01, −2	1.25, −1	1.07, −2
90	2.68, −1	5.62, −2	7.02, −1	9.33, −3	1.18, −1	9.57, −3
100	2.45, −1	5.15, −2	6.72, −1	8.67, −3	1.11, −1	8.71, −3
150	1.72, −1	3.62, −2	5.35, −1	6.36, −3	9.05, −2	5.94, −3
200	1.33, −1	2.79, −2	4.50, −1	5.02, −3	7.50, −2	4.46, −3
300	9.20, −2	1.91, −2	3.51, −1	3.53, −3	5.74, −2	3.02, −3
350	7.98, −2	1.65, −2	3.14, −1	3.08, −3	5.19, −2	2.59, −3
400	7.06, −2	1.45, −2	2.85, −1	2.73, −3	4.74, −2	2.27, −3
500	5.73, −2	1.17, −2	2.39, −1	2.22, −3	4.01, −2	1.81, −3
680	4.29, −2	8.67, −3	1.99, −1	1.66, −3	3.29, −2	1.35, −3
1000	2.96, −2	5.94, −3	1.44, −1	1.15, −3	2.36, −2	9.12, −4

[a] $1.01,-1 \equiv 1.01 \times 10^{-1}$.

a vertical broken line in that figure. Callaway (1985) has performed other calculations with the algebraic variational close-coupling method (AVCC) using a smaller (11-state) pseudostate basis set. The primary difference between Callaway's 11-state AVCC calculation and his 18-state optical model calculation (Callaway *et al* 1987) is the inclusion of all the $n = 3$ states exactly within the $\mathcal{P}$ subspace, improving the handling of the partial waves with $L \geq 4$, and the characterization of continuum d states. The latter two points have been discussed in detail by van Wyngaarden and Walters (1986a). They conclude that Callaway's 11-state AVCC results for the $\sigma_{1s\to 2p}$ cross section are an overestimation at 54.40 eV, and propose revising the 11-state AVCC results for the $\sigma_{1s\to 2p}$ cross section to bring it into agreement with their own pseudostate calculations (van Wyngaarden and Walters 1985, 1986b). The revised $\sigma_{1s\to 2p}$ cross section of van Wyngaarden and Walters, and the original 11-state AVCC results of Callaway are compared in figure 2 with the present DMET results and the 18-state results of Callaway *et al.* The DMET results and the 11-state AVCC results of Callaway are in agreement with the absolute measurement of Williams (1981) at $E = 54.40$ eV, while the revised

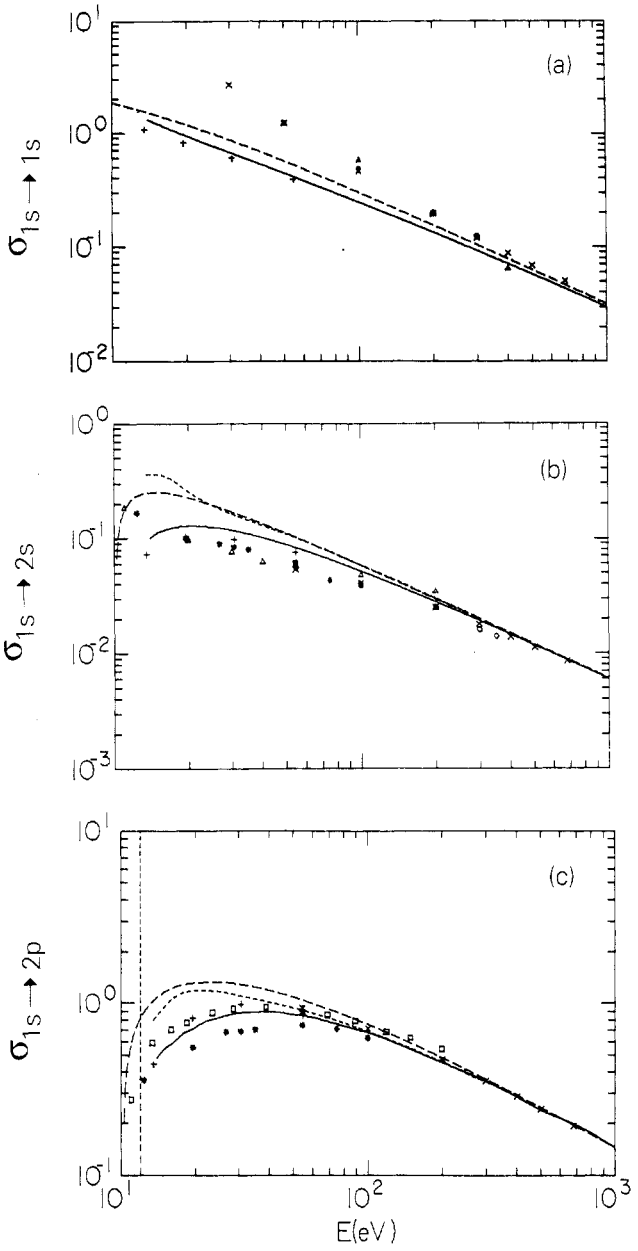

Figure 1. (*a*)–(*c*) Integral cross sections: (*a*) $\sigma_{1s\rightarrow 1s}$, (*b*) $\sigma_{1s\rightarrow 2s}$ and (*c*) $\sigma_{1s\rightarrow 2p}$ (all in πa_0^2). Long broken curve, first Born result; full curve, present DMET result; +, unitarized Born results (Somerville 1963); ×, DWSBA results (Kingston and Walters 1980). In (*a*): ⋆, pseudostate results (van Wyngaarden and Walters 1986b); △, experimental data of Williams (1975) as integrated by de Heer *et al* (1977). In (*b*): short broken curve, 3-state close-coupling results (Kingston *et al* 1976); ⋆, 18-state optical potential results (Callaway *et al* 1987); △, experimental data of Kauppila *et al* (1970) as renormalized by Callaway and McDowell (1983); ○, experimental data of Kauppila *et al* (1970) as renormalized by van Wyngaarden and Walters (1986b). In (*c*): △, experimental data of Williams (1981) at 54.40 eV; □, experimental data of Long *et al* (1968) as renormalized by Bransden and McDowell (1978).

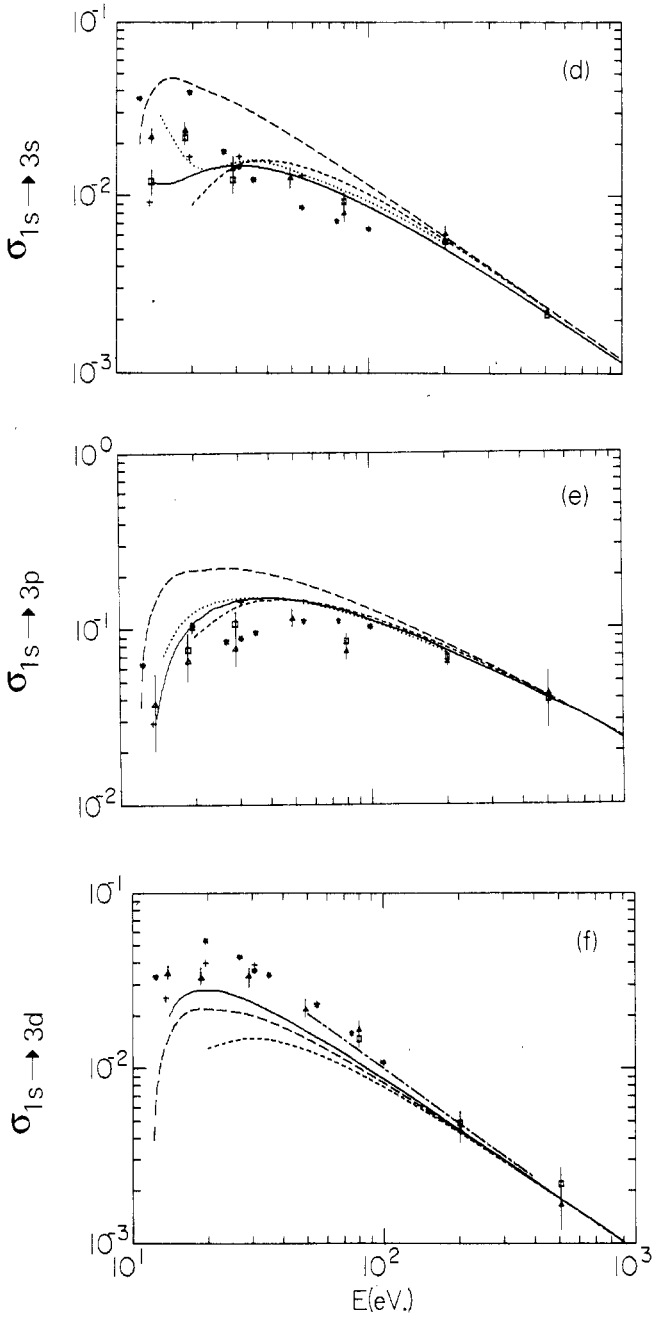

Figure 1. (*d*)–(*f*) Integral cross sections: (*d*) $\sigma_{1s\rightarrow 3s}$, (*e*) $\sigma_{1s\rightarrow 3p}$ and (*f*) $\sigma_{1s\rightarrow 3d}$ (all in πa_0^2). All symbols are the same as figures 1(*a*)–(*c*) except where noted. Short broken curve, Glauber theory (Chan and Chang 1977); dotted curve, DWPO-II results (Syms *et al* 1975); △, experimental in-phase plus out-of-phase data (Mahan *et al* 1976, table 1); □, experimental in-phase data only (Mahan *et al* 1976, table 1). Note that in (*d*) the data point of Mahan *et al* at 13.8 eV taken from their table 1 does not agree with their figure 8. All data of Mahan *et al* are taken from their table 1. In (*f*): chain curve, SODM (Baye and Heenen 1974).

cross section of van Wyngaarden and Walters and the 18-state optical model results of Callaway *et al* fall below Williams's result at 54.40 eV by 20%. The experimental results of Long *et al*, as renormalized by Bransden and McDowell (1978) at 11 eV, are also shown in figure 2. The absolute measurement of Williams at 54.40 eV is in accord with the renormalization of Bransden and McDowell. However, van Wyngaarden and Walters (1986a, b) have argued that the measurements of Long *et al* should be renormalized at $E = 200$ eV in order to reproduce their pseudostate results at 200 eV. The experimental results of Long *et al*, as renormalized by van Wyngaarden and Walters at 200 eV are also shown in figure 2. The high-energy renormalization of the data of Long *et al* clearly favours the 18-state results of Callaway *et al*.

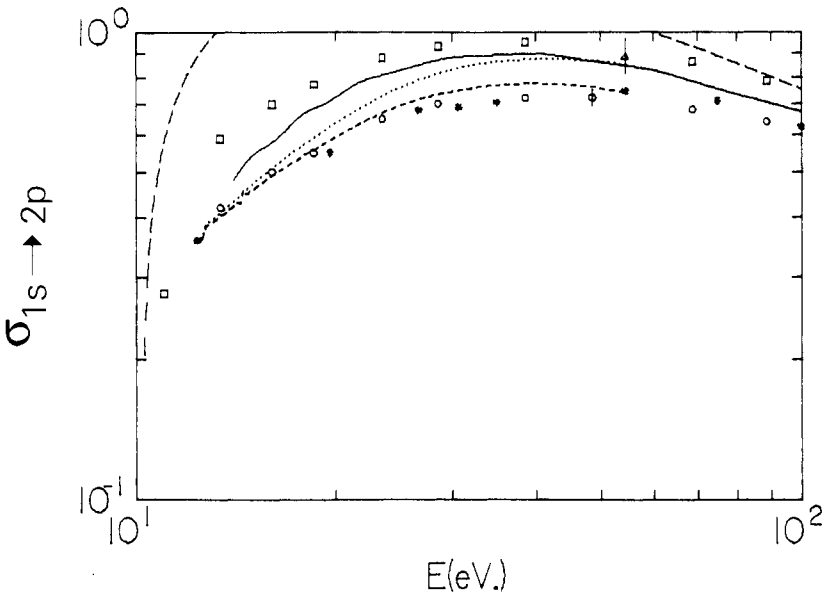

Figure 2. Blow-up of figure 1(*c*) from threshold to 100 eV. All symbols are the same as in figure 1(*c*) except where noted. Dotted curve, 11-state AVCC results (Callaway 1985); short broken curve, 11-state AVCC results (Callaway 1985) as renormalized by van Wyngaarden and Walters (1986a); *, 18-state optical potential results (Callaway *et al* 1987); □, experimental data (Long *et al* 1968) as renormalized by Bransden and McDowell (1978); ○, experimental data (Long *et al* 1968) as renormalized by van Wyngaarden and Walters (1986a); △, experimental data of Williams (1981) at 54.40 eV.

Indeed the issue of how to reduce the relative measurements of Kauppila *et al* and Long *et al* to an absolute scale relies upon knowing the integral cross sections for excitation of states nl of H, with principal quantum number $n = 3, 4$ and 5. Knowledge of such cross sections is required for the calculation of the cascade contribution to the $\sigma_{1s \rightarrow 2s}$ and $\sigma_{1s \rightarrow 2p}$ cross sections and, more importantly, when compared with experimental data provides an important check of one of the central assumptions of all the pseudostate calculations previously discussed. In partitioning a set of basis states characterizing the target atom into $\mathcal{P}$ and $\mathcal{Q}$ subspaces, comprising states one is explicitly interested in computing the cross sections for (the $\mathcal{P}$ subspace), with (pseudo)states chosen to model the infinite number of states necessarily omitted from any calculation (the $\mathcal{Q}$ subspace), one assumes that the division of states between the

$\mathcal{P}$ and $\mathcal{Q}$ subspaces is done in such a way so that the remaining dynamical couplings between the $\mathcal{Q}$ subspace states are weak.

Overall, the agreement between the DMET results and the experimental data of Mahan *et al* (1976) is very encouraging, especially for the 1s → 3s and 1s → 3d transitions (see figures 1(*d*)-(*f*)). Note that for clarity both data points of Mahan *et al* are shown in figures 1(*d*)-(*f*) at each energy only if they are clearly distinguishable. In all three cases the DMET results clearly have converged to the Born result for $E \geq 500$ eV. In contrast, the 18-state optical model results of Callaway *et al* for the $\sigma_{1s\rightarrow 3s}$ cross section would seem to be too low in the energy range from 30 to 100 eV, and appear to be having difficulty converging to the Born at high energies. Also, the 18-state optical model results of Callaway *et al* appear to overestimate the $\sigma_{1s\rightarrow 3s}$ and $\sigma_{1s\rightarrow 3d}$ cross sections in the energy range from threshold to about 30 eV when compared with the experimental results of Mahan *et al*. The 18-state results of Callaway for the $\sigma_{1s\rightarrow 3p}$ cross section, however, are in good agreement with the experimental data of Mahan *et al* in the range from 30 to 100 eV. Overall however, the trend of the DMET results in figures 1(*d*)-(*f*) and the experimental data of Mahan *et al* would seem to indicate that the optical potential method of Callaway *et al* (1987) needs refinement in the energy range from threshold to about 30 eV.

In addition, the assumption in the pseudostate calculations that the dynamical couplings between states in the $\mathcal{Q}$ subspace is weak should be investigated in more detail, particularly for the case of the 1s → 3d transition. An estimate of the importance of couplings within the $n = 4$ manifold of states and between the $n = 3$ and $n = 4$ states can be obtained by comparing the DMET results with the important second-order diagonalization method (SODM) results of Baye and Heenen (1974) in figure 1(*f*). The SODM results of Baye and Heenen are 21% above the DMET results for the $\sigma_{1s\rightarrow 3d}$ cross section at $E = 50$ eV, and are in excellent agreement with the experimental data of Mahan *et al* for $E \geq 50$ eV. In fact, it would appear from figure 1(*f*), that the dynamical couplings to and within the $n = 4$ manifold of states of H have a sizable influence on the $\sigma_{1s\rightarrow 3d}$ cross section for energies E≤ 100 eV, an influence which increases with decreasing energy.

The most important trend observed by Mahan *et al* in their experimental data is that the Born cross section for the 1s → 3d transition lies *below* the measured values for energies near threshold by nearly a factor of two. This is opposite to the trend observed in s → p transitions where the first Born results always lie above the measured values in the intermediate energy range. The reversal of trends in s → d transitions, observed by Mahan *et al*, was first predicted by Somerville (1963) in a pioneering unitarized Born calculation a decade before the experimental measurements of Mahan *et al* (1976). Recently, Whelan (1986) has updated and extended the unitarized Born calculations of Somerville, confirming the trend in s → d transitions seen in the original calculations of Somerville. The physical reason for such a trend in the cross section for s → d transitions lies in the principle of conservation of flux. In the unitarized Born calculations of Somerville, flux is conserved exactly for all energies; whereas numerical inaccuracies in the present calculations, due to the breakdown of the assumption of straight-line trajectories for small impact parameters $\rho \leq 0.20a_0$ (Mansky 1990a), results in the sum of the probabilities for exciting each of the states in the basis set departing from unity by an amount ≤ 10% for all energies between 14 and 1000 eV, and by ≤ 4% for energies $E \geq 20$ eV. Hence, as target states with higher principal quantum number n are included in a basis set, the strong multipole moments which couple these states together result in increasing the possibility that indirect excitation mechanisms

such as 1s → 2p → 3d and 1s → 3p → 3d will occur. Therefore, theories which regard the scattering event as proceeding via a direct excitation of the final state from the initial state, as the first Born does, will tend to underestimate the cross section in the energy range where a large number of indirect channels for excitation are open. Other theories which invoke a direct mechanism for the excitation of the 3d state, and predict cross sections $\sigma_{1s\rightarrow 3d}$ which are too low compared with the experimental results of Mahan *et al*, include the distorted-wave polarized orbital approximation (DWPO) of Syms *et al* (1975), and the Glauber theory results of Chan and Chang (1977). For clarity only the Glauber results of Chan and Chang are shown in figure 1(*f*). Another manifestation of the inclusion of indirect channels in the excitation of the 3d state of H involves the polarization properties of the photons emitted in the decay of the 3d state, and will be discussed in section 3.3.

For completeness, the cross section for excitation of Balmer Hα

$$\sigma(\mathrm{H}\alpha) = \sigma_{1s\rightarrow 3s} + 0.118\sigma_{1s\rightarrow 3p} + \sigma_{1s\rightarrow 3d}$$

is shown in figure 3. The DMET results are in excellent agreement with the experimental data of Mahan *et al* for all but the lowest energy (13.8 eV). Also shown in figure 3 are the 18-state optical model results of Callaway *et al*, which agree closely with the DMET results for $E \geq 30$ eV, but which tend to overestimate the cross section at lower energies. Again, a refinement of the optical potential used by Callaway *et al* (1987) for energies near threshold may be warranted.

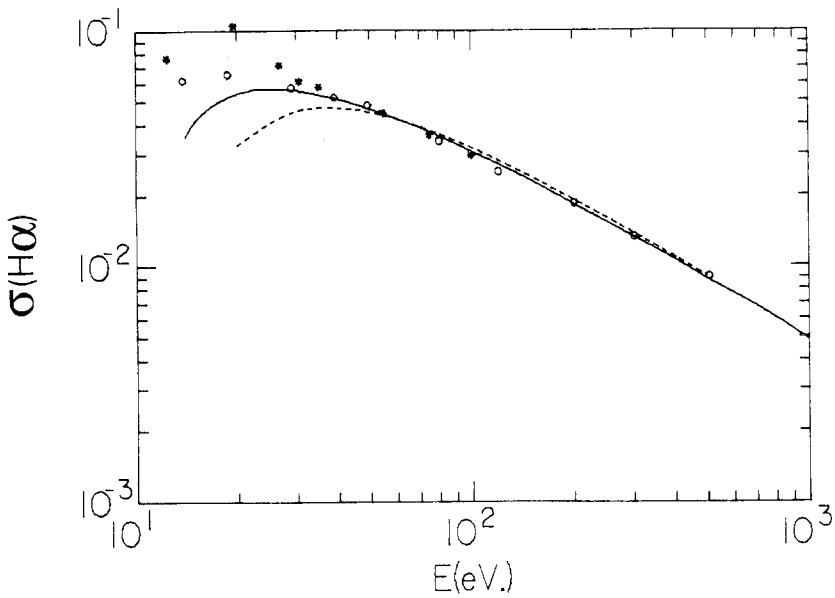

Figure 3. Integral cross section σ(Hα) for Balmer Hα emission (in πa_0^2). Full curve, present DMET results; short broken curve, Glauber theory (Chan and Chang 1977); long broken curve, first Born result; *, 18-state optical potential results (Callaway *et al* 1987); O, experimental data (Mahan *et al* 1976).

For a more detailed discussion of the DMET results for the $\sigma_{1s\rightarrow 2s}$ and $\sigma_{1s\rightarrow 2p}$ integral cross sections for energies $E \leq 100$ eV, as well as a comparison with the

recent intermediate energy R-matrix (IERM) results of Scott *et al* (1989), see Mansky and Flannery (1990). The IERM results of Scott *et al* (1989) are in quantitative agreement with the 18-state results of Callaway *et al* and the multipseudostate results of van Wyngaarden and Walters (1986b). We also note that the DMET expression in (10) for the complex scattering amplitude satisfies the optical theorem. A comparison of the DMET and AVCC predictions for the total inelastic integral cross section is also given in Mansky and Flannery (1990).

3.2. Differential cross sections

An overview of the DMET results for the H differential cross sections is given in figure 4, while a more detailed tabulation is given in Mansky (1990b). Data at other energies and angles are available upon request.

In this paper we are particularly concerned with assessing the accuracy of the DMET integral cross section, therefore we will concentrate on examining the DMET differential cross sections in the forward direction, $0° \leq \theta \leq 40°$, only. Due to the appearance of the diffraction-like Bessel functions in (1) rather than the Legendre polynomials and the neglect of electron exchange in the present calculations, the DMET differential cross sections are expected to underestimate the experimental results for electron scattering angles $\theta \geq 40°$. This is most clearly shown in figure 4(a) where the DMET elastic differential cross section is compared with the experimental data of Williams (1975). As expected, the DMET differential cross section (DCS) for the elastic channel is accurate in the forward direction only for energies ≥ 100 eV due to the neglect of polarization distortion and electron exchange in the elastic channel.

The DMET DCS results for the 1s $\rightarrow$ 2s and 1s $\rightarrow$ 2p transitions are compared with the 3-state close-coupling results of Kingston *et al* (1976) and the pseudostate calculations of van Wyngaarden and Walters (1986b) in figure 5. Also shown in figures 5(a) and (b) are the absolute measurements of Williams (1981). The overall agreement between the DMET results and the experimental data of Williams is quite good for angles $\theta \leq 40°$. Interestingly, the DMET DCS results in figure 5 lie closer to the close-coupling results of Kingston *et al* for scattering angles $\theta \leq 40°$. For larger angles, $\theta \geq 40°$, the influence of electron exchange is clearly evident by the rapid decline of the DMET results compared with the results of Kingston *et al* and van Wyngaarden and Walters, both of which include exchange. For clarity, only a selection of theoretical results have been shown in figure 5. A fuller quantitative comparison of the DMET results at $E = 54.40$ eV for the 1s $\rightarrow$ 2s and 1s $\rightarrow$ 2p DCS is given in tables 2 and 3 respectively. Also, for completeness, the DMET results for the summed DCS for the 1s $\rightarrow$ 2s + 2p transition are compared with the experimental results of Williams and Willis (1975) in figure 6. Loss of accuracy in the DMET DCS results for the 1s $\rightarrow$ 2p and 1s $\rightarrow$ 3p dipole channels is indicated by the appearance, at large scattering angles $\theta \geq 30°$, of small oscillations at high energies. This is a result of the use of the diffractive-like Bessel functions in the DMET which is valid only for scattering into the angular region $\theta \leq (ka)^{-1}$ where a is the effective range. As k increases, the Bessel function variation at larger scattering angles does not reproduce the correct $P_l(\theta)$ variation predicted by partial wave expansions used in close-coupling theories.

The dipole correction (10a) to the scattering amplitude has only a small influence on the integral cross sections, amounting to an increase of only $\frac{1}{4}$% at 54.40 eV, and increasing to 1.4% at 1000 eV for $\sigma_{1s\rightarrow 2p}$. However, the dipole correction has a sizable influence on the DCS for the inelastic transitions 1s $\rightarrow$ 2p and 1s $\rightarrow$ 3p in the forward direction. For example, inclusion of the dipole correction in the 1s $\rightarrow$ 2p transition

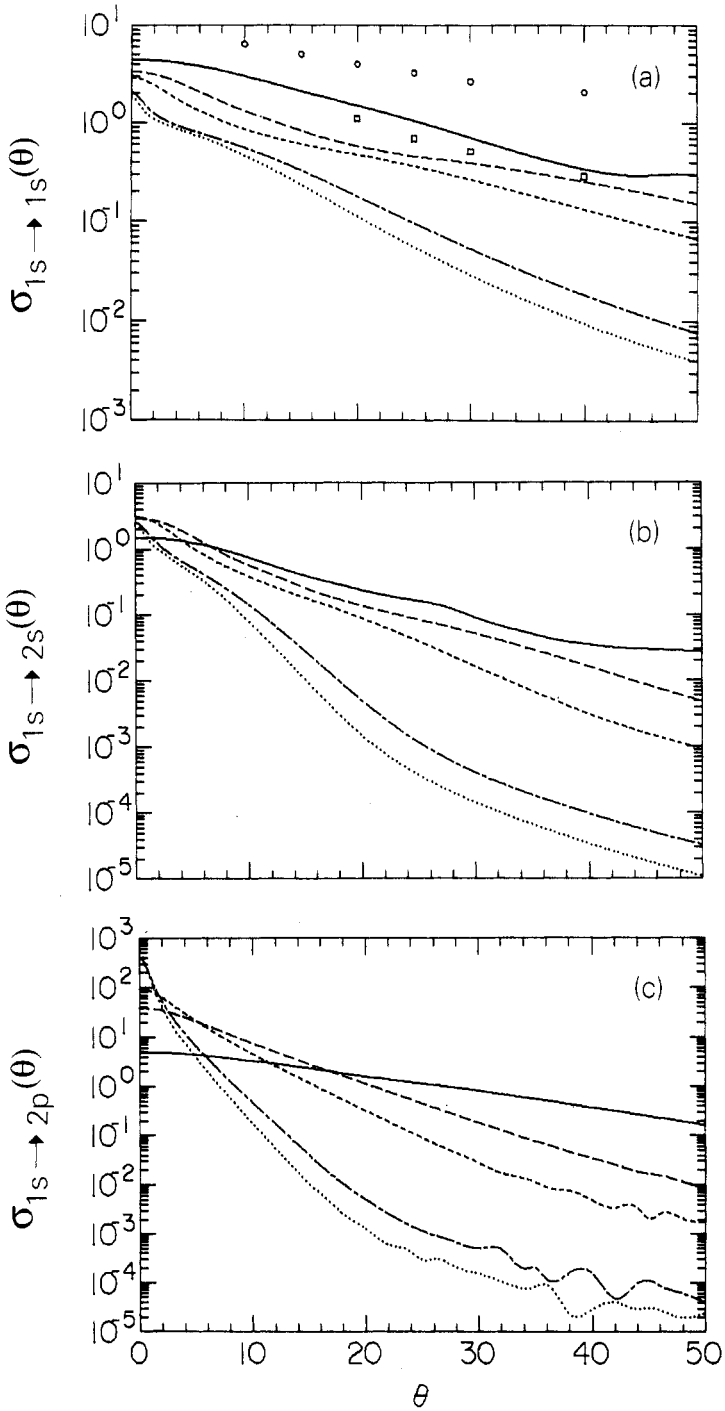

Figure 4. (*a*)-(*c*) Differential cross sections: (*a*) $\sigma_{1s\rightarrow 1s}(\theta)$, (*b*) $\sigma_{1s\rightarrow 2s}(\theta)$ and (*c*) $\sigma_{1s\rightarrow 2p}(\theta)$ (all in a_0^2 sr^{-1}). Present DMET results at 20, 54.40, 100, 350 and 500 eV denoted by a full curve, long broken curve, short broken curve, chain curve and dotted curve, respectively. In (*a*): ○, □, experimental data (Williams 1975) at 20 and 100 eV, respectively.

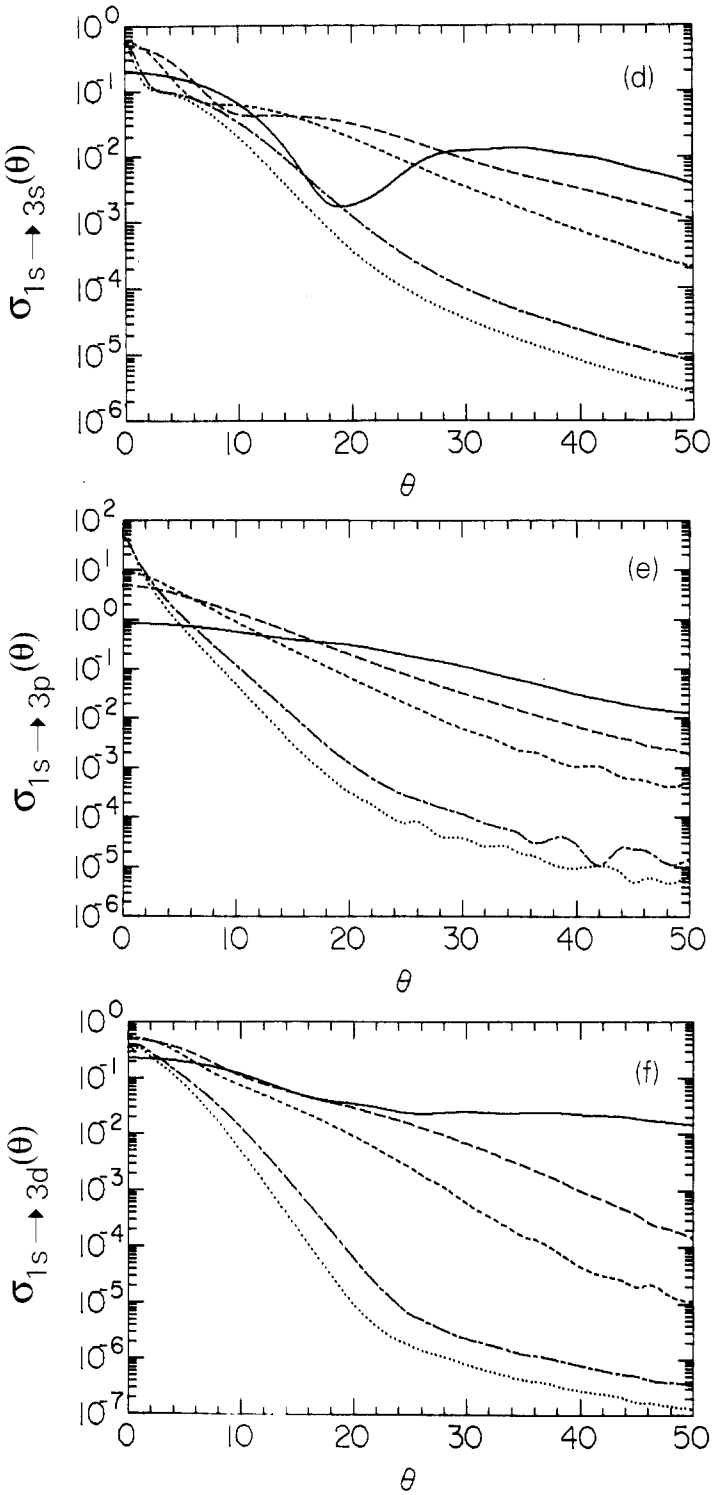

Figure 4. (*d*)–(*f*) Differential cross sections: (*d*) $\sigma_{1s\rightarrow 3s}(\theta)$, (*e*) $\sigma_{1s\rightarrow 3p}(\theta)$ and (*f*) $\sigma_{1s\rightarrow 3d}(\theta)$ (all in a_0^2 sr^{-1}). All symbols are the same as in figures 4(*a*)–(*c*).

Table 2. Comparison of theoretical and experimental values of $\sigma_{1s\rightarrow 2s}(\theta)$ (a_0^2 sr^{-1}) for $E = 54.40$ eV.

θ	DMET	DWSBA[a]	CC[b]	CC[c]	CCOM[d]	EIK[e]	Exp-1[f]	Exp-2[g]
0	2.93	1.63	3.26	1.85	2.9	1.96		
2	2.62	1.43		1.64		1.83		
4	1.92	1.03		1.20		1.54		
6	1.24	6.81, −1		8.17, −1		1.21		
8	8.02, −1	4.60, −1		5.56, −1		9.13, −1		
10	5.58, −1	3.33, −1	5.75, −1	3.93, −1	5.6, −1	6.78, −1	3.80,−1±1.28,−1	5.94,−1±0.94,−1
12	4.07, −1	2.57, −1		2.90, −1		4.96, −1		
14	2.94, −1	2.07, −1		2.21, −1		3.57, −1		
16	2.15, −1	1.69, −1		1.71, −1		2.55, −1		
18	1.67, −1	1.37, −1		1.33, −1		1.80, −1		
20	1.34, −1	1.10, −1	1.23, −1	1.03, −1	9.8, −2	1.27, −1	9.0, −2±1.8,−2	1.16, −1±0.17,−1
30	5.12, −2	2.70, −2	4.43, −2	2.72, −2	3.0, −2	3.16, −2	3.5, −2±0.39,−2	3.75, −2±0.40,−2
35	2.94, −2	1.24, −2		1.50, −2				
40	1.61, −2	6.9 , −3	1.90, −2	9.97, −3	1.19, −2		1.65, −2±1.28,−2	1.84, −2±0.47,−2

[a] Distorted-wave second Born approximation results of Kingston and Walters (1980).
[b] Three-state close-coupling results of Kingston *et al* (1976).
[c] Close-coupling pseudostate results of van Wyngaarden and Walters (1986b).
[d] Six-state coupled channels optical model results of McCarthy and Stelbovics (1983).
[e] Second-order eikonal results of Unnikrishnan and Prasad (1982).
[f] Experimental results of Williams (1981) using the sum $\sigma_{1s\rightarrow 2s}(\theta) + \sigma_{1s\rightarrow 2p}(\theta)$.
[g] Experimental results of Williams (1981) using the ratio $\sigma_{1s\rightarrow 2s}(\theta)/\sigma_{1s\rightarrow 2p}(\theta)$.

Table 3. Comparison of experimental and theoretical values of $\sigma_{1s\rightarrow 2p}(\theta)(a_0^2\ \mathrm{sr}^{-1})$ for $E = 54.40$ eV.

θ	DMET	MET	DWSBA[a]	CC[b]	CC[c]	CCOM[d]	EIK[e]	SODW[f]	Exp[g]
0	3.85,+1	3.33,+1	4.63,+1	3.90, +1	3.74, +1	3.8, +1	4.10, +1	4.303, +1	
2	3.38,+1	3.08,+1	4.10,+1	3.31, +1		3.61, +1			
4	2.46,+1	2.46,+1	3.01,+1	2.41, +1		2.59, +1			
6	1.66,+1	1.74,+1	2.03,+1	1.60, +1		1.69, +1			
8	1.10,+1	1.14,+1	1.32,+1	1.02, +1		1.06, +1			
10	7.31	7.22	8.57	7.81	6.51	6.9	6.61	7.918	7.54±0.71
12	4.94	4.81	5.56		4.14		4.13		
14	3.38	3.35	3.61		2.64		2.59		
16	2.32	2.34	2.34		1.69		1.63		
18	1.60	1.62	1.51		1.09		1.03		
20	1.11	1.11	9.64,−1	1.18	7.02,−1	9.7, −1	6.49,−1	9.498,−1	1.04±0.11
30	1.79,−1	1.79,−1	9.69,−2	1.99,−1	9.89,−2	1.62,−1	7.56,−2	1.182,−1	1.57,−1±0.21,−1
35	7.48,−2	7.48,−2	3.61,−2	4.97,−2	5.201,−2				
40	3.37,−2	3.37,−2	1.98,−2	4.71,−2	3.15,−2	4.2, −2		3.047,−2	4.36,−2±0.69,−2
$\sigma\ (a_0^2)$	2.65	2.65	2.963	2.853	2.322	2.55			2.79 ±0.24

[a] Distorted-wave second Born approximation results of Kingston and Walters (1980).
[b] Three-state close-coupling results of Kingston *et al* (1976).
[c] Close-coupling pseudostate results of van Wyngaarden and Walters (1986b).
[d] Six-state coupled channels optical model results of McCarthy and Stelbovics (1983).
[e] Second-order eikonal results of Unnikrishnan and Prasad (1982).
[f] Second-order distorted-wave results of Madison *et al* (1985).
[g] Experimental results of Williams (1981).

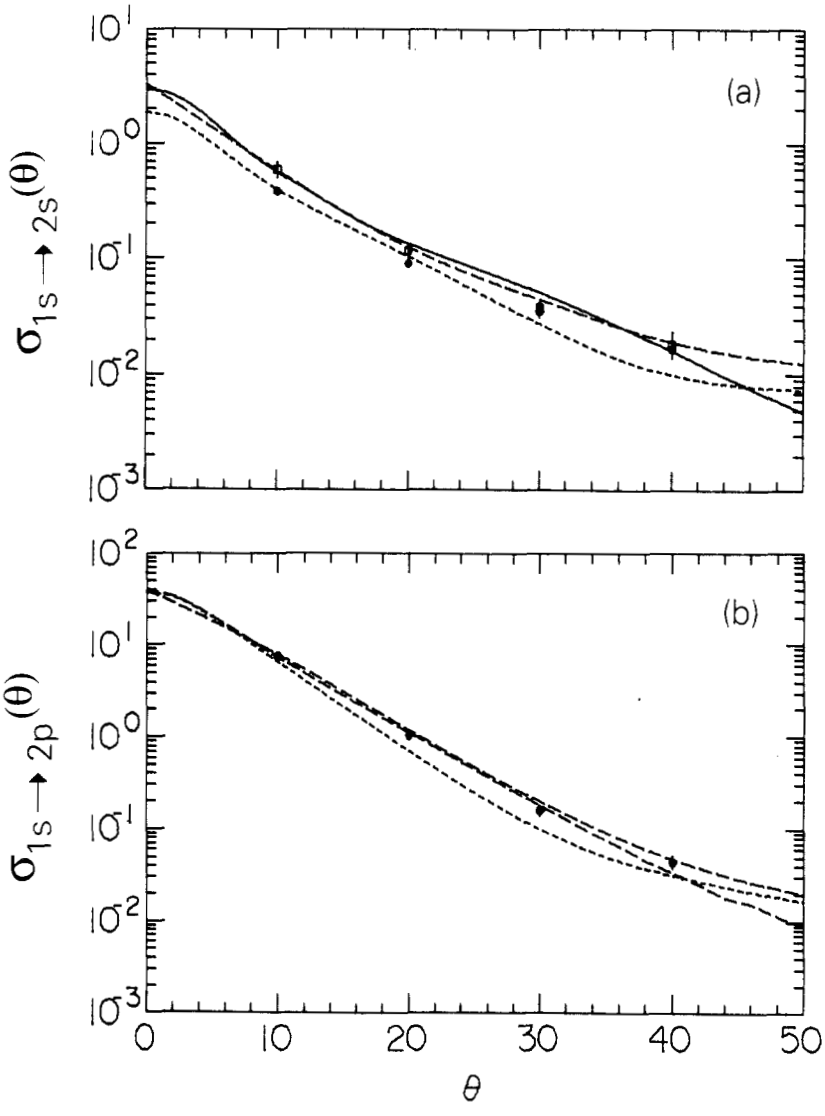

Figure 5. Differential cross sections: (*a*) $\sigma_{1s \rightarrow 2s}(\theta)$ and (*b*) $\sigma_{1s \rightarrow 2p}(\theta)$ at E = 54.40 eV (in a_0^2 sr^{-1}). Full curve, present DMET results; long broken curve, 3-state close-coupling results (Kingston *et al* 1976); short broken curve, pseudostate results (van Wyngaarden and Walters 1986b); ○, experimental data (Williams 1981) via DCS sum; □, experimental data (Williams 1981) via DCS ratio.

results in an increase in the DCS at $\theta = 0°$ of 15.6% at E = 54.40 eV and 57% at E = 1000 eV. When (10*a*) is applied to the 1s → 3p transition, the MET DCS at $\theta = 0°$ is increased by 6.8% and 38% at E = 54.40 and 1000 eV, respectively. The reason the dipole corrections in the DMET have a much smaller effect on integral cross sections $\sigma_{1s \rightarrow 2p}$ and $\sigma_{1s \rightarrow 3p}$ than on the corresponding differential cross sections is due to the appearance of the $\sin(\theta)$ weighting factor in equation (4*b*).

The most interesting trend observed in the DMET DCS results is the occurrence of a minimum in the inelastic 1s → 3s DCS. The minimum is most pronounced at

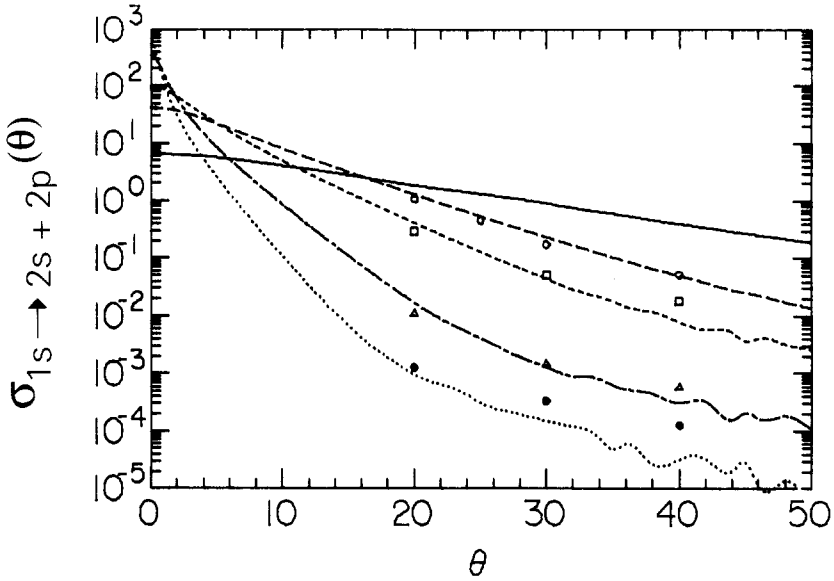

Figure 6. Composite differential cross section $\sigma_{1s\rightarrow 2s+2p}(\theta) \equiv \sigma_{1s\rightarrow 2s}(\theta) + \sigma_{1s\rightarrow 2p}(\theta)$ in a_0^2 sr^{-1}. Present DMET results at 20, 54.40, 100, 300 and 680 eV are denoted by a full curve, long broken curve, short broken curve, chain curve and dotted curve, respectively. ○, □, △ and ●, experimental data (Williams and Willis 1975) at 54.40, 100, 300 and 680 eV, respectively.

$E = 20$ eV where it occurs at $\theta = 20°$, but clearly persists at higher energies and shifts inwards, occurring at angles of 10° and 2° for energies of 100 and 500 eV, respectively. A much broader and shallower minimum is observed in the DMET DCS results for the 1s → 3d at $E = 20$ eV. The appearance of the minima in the DMET DCS results for the 1s → 3s and 1s → 3d transitions, is due physically to the increase in the number of competing indirect mechanisms for the excitation of the $3l$ states of H. Thus, the scattering amplitudes for excitation of the higher states in the basis set, especially for optically forbidden transitions, are particularly sensitive functions of the relative strength of the various multipole interactions which couple (in an off-diagonal manner) the states in the basis set together. Hence, the resulting DCS exhibit minima and maxima as seen in figure 4(*d*).

3.3. Polarization properties

In addition to the differential and integral cross sections, which provide a measure of the scattering properties of and the excitation probabilities within the target basis set, analysis of the polarization properties of the photons emitted in the decay of the 2p, 3p and 3d states of H will provide a direct measure of the moduli and relative phases among the scattering amplitudes for excitation of the $2p_m$, $3p_m$ and $3d_m$ magnetic substates. This will give information about the orientation and alignment of the charge cloud of the excited states after the scattering event, as well as the relative proportions of linear compared with circularly polarized light emitted in the decay of the metastable states. The theory required for the analysis of the polarization properties of emitted radiation is well developed (Macek and Jaecks 1971, Fano and Macek 1973, Blum and Kleinpoppen 1979, Hertel *et al* 1985 and Andersen *et al* 1988).

This paper is confined to the analysis of the decay of the 2p state at two energies (54.40 and 350 eV) where experiments have been performed. A detailed state multipole analysis of the 2p, 3p and 3d states of hydrogen will be reported separately (Mansky 1990b).

In figures 7(*a*)–(*c*) the DMET results for the $\lambda(2p)$, $R(2p)$ and $I(2p)$ parameters are compared with the close-coupling results of Kingston *et al* (1982) and the pseudostate calculations of van Wyngaarden and Walters (1986b) for an incident electron energy of 54.40 eV. The λ, R and I parameters allow for a complete determination of the coincident rate between the scattered electron and the emitted photon, and are defined (Morgan and McDowell 1975)

$$\lambda(2p) = |f_0|^2/(|f_0|^2 + |f_{\pm 1}|^2) \tag{11a}$$

$$R(2p) = \sqrt{(\tfrac{1}{2})\lambda(1-\lambda)}\cos(\chi) \tag{11b}$$

$$I(2p) = \sqrt{(\tfrac{1}{2})\lambda(1-\lambda)}\sin(\chi) \tag{11c}$$

where $\chi = \beta_{+1} - \beta_0$, and $f_m = |f_m|e^{i\beta_m}$, with f_m denoting the complex scattering amplitude for the excitation of the $2p_m$ magnetic substates. The experimental data shown in figures 7(*a*) and (*b*) are the absolute measurements of Williams (1981), and in figure 7(*c*), those of Williams (1986). Clearly, while the DMET results for the $1s \rightarrow 2p$ DCS are in good agreement with the experiment for $\theta \leq 40°$ (compare figure 7(*a*) with figure 5(*b*)), the DCS for the individual $2p_m$ substates are quite different. The close-coupling results of Kingston *et al* (1982) and the pseudostate calculation of van Wyngaarden and Walters (1986b) predict a $\lambda(2p)$ parameter in better agreement with experiment for scattering angles $\theta \leq 40°$. However, to date, *no* theory has predicted values for all three parameters in agreement with experiment at *all* scattering angles. The primary theoretical difficulty has been in obtaining a minimum in the λ parameter at $\theta \sim 100°$ of sufficient depth, while predicting an R parameter which becomes sufficiently negative for scattering angles $\theta \geq 80°$. In this regard, it is interesting to note that the DMET results for the R parameter *always* becomes negative over some angular range for all incident energies studied. For example, letting θ_0 = electron scattering angle at which the $R(2p)$ parameter first passes through zero and becomes negative, then the DMET results predict that $\theta_0 = 36°, 26°, 16°$ and $10°$ for energies of 54.40, 100, 350 and 500 eV, respectively. Clearly, electron exchange is not required to predict a negative R parameter. At higher energies and smaller electron scattering angles, the influence of electron exchange should be significantly reduced, thereby providing a better regime for testing the accuracy of the DMET results. In figure 8 the DMET results for the λ, R and I parameters at 350 eV are compared with the pseudostate calculations of van Wyngaarden and Walters (1986b), and the recent experimental data of Williams and Heck (1988). While both theories predict similiar trends for the parameters, neither is successful in reproducing all the experimental data.

4. Conclusions

The principal aim of this paper was to test the DMET results for the inelastic $1s \rightarrow 2l$ and $1s \rightarrow 3l$ transitions against the available experimental and theoretical data. In

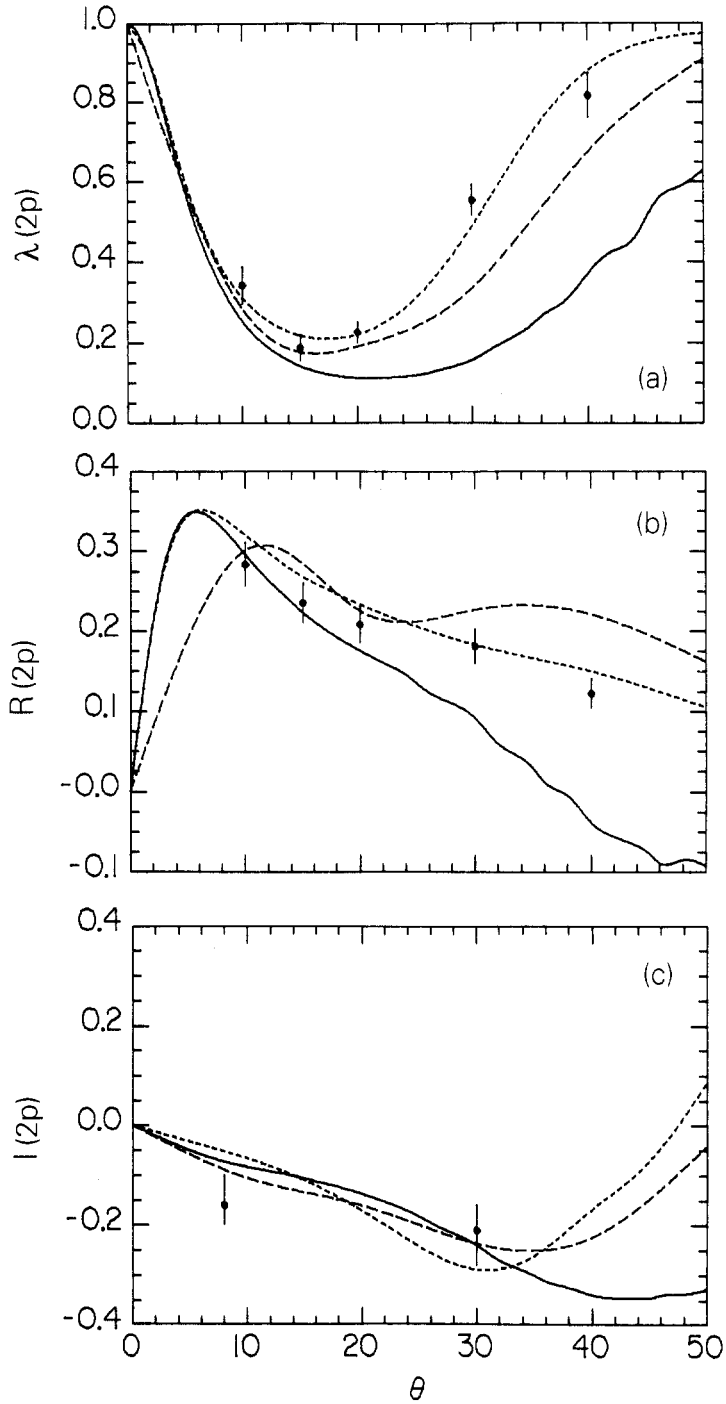

Figure 7. λ, R and I parameters for the 2p state of H at 54.40 eV. Full curve, present DMET results; long broken curve, 3-state close-coupling results (Kingston *et al* 1976); short broken curve, pseudostate results (van Wyngaarden and Walters 1986b). In (*a*) and (*b*): O, experimental data (Williams 1981). In (*c*): O, experimental data (Williams 1986).

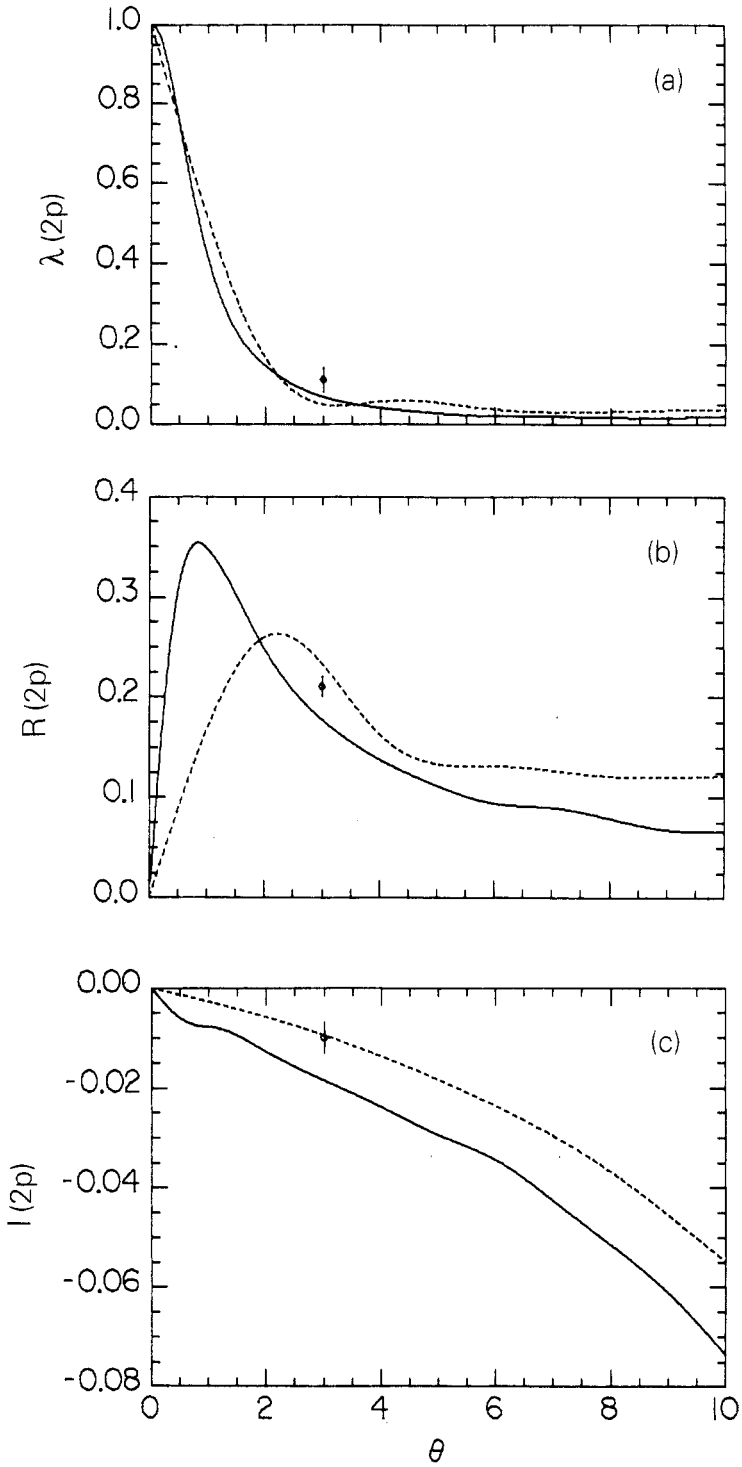

Figure 8. Same as figure 7 except for $E = 350$ eV. All symbols are the same as in figure 7 except where noted. O, experimental data (Williams and Heck 1988).

the case of the 1s → 2s and 1s → 2p transitions, the agreement between the DMET results and the available theoretical and experimental data is satisfactory. However, the theoretical issue of which low-energy/high-energy renormalization of the experimental data of Long *et al* (1968) for the 1s → 2p integral cross section is to be preferred requires, for resolution, both inclusion of full polarization distortion and electron exchange effects, and (for theories employing an optical potential) careful examination of the basis states used in the calculation so that the states within the $\mathcal{P}$ subspace are chosen such that all important couplings that can appreciably influence the 1s → 2s and 1s → 2p transitions are included, and the remaining dynamical couplings within the $\mathcal{Q}$ subspace are indeed weak.

That is, in the case of the 1s → 2s and 1s → 2p transitions in H, inclusion of the strong 2s → 2p and $2l \rightarrow 3l'$ intermediate couplings are important for all theories (including optical potential theories).

In the case of the 1s → $3l$ transitions, the DMET results are in good overall agreement with the experimental data of Mahan *et al* (1976). The DMET results for the $\sigma_{1s\rightarrow 3d}$, when compared with the unitarized Born results of Somerville (1963), clearly show the importance of indirect, or higher-order, mechanisms in the excitation of the 3d state. This has an important consequence in that the integral cross section for the 1s → 3d transition *exceeds* the Born result in the intermediate energy region.

Acknowledgments

This research is supported by US Air Force Office of Scientific Research under Grant No AFOSR-89-0426.

References

Andersen N, Gallagher J W and Hertel I V 1988 *Phys. Rep.* **165** 1–188
Baye D and Heenen P-H 1974 *J. Phys. B: At. Mol. Phys.* **7** 928–37
Blum K and Kleinpoppen H 1979 *Phys. Rep.* **52** 203–61
Bransden B H and McDowell M R C 1978 *Phys. Rep.* **46** 249–394
Burgess D D, Kolbe G and Ward J M 1978 *J. Phys. B: At. Mol. Phys.* **11** 2765–78
Burgess D D, Myerscough V P, Skinner C H and Ward J M 1980 *J. Phys. B: At. Mol. Phys.* **13** 1675–701
Callaway J 1982 *Phys. Rev.* A **26** 199–208
—— 1985 *Phys. Rev.* A **32** 775–83
Callaway J and McDowell M R C 1983 *Comment. At. Mol. Phys.* **13** 19–35
Callaway J and Oza D H 1985 *Phys. Rev.* A **32** 2628–36
Callaway J, Unnikrishnan K and Oza D H 1987 *Phys. Rev.* A **36** 2576–84
Chan F T and Chang C H 1977 *Phys. Rev.* A **15** 118–27
de Heer F J, McDowell M R C and Wagenaar R W.1977 *J. Phys. B: At. Mol. Phys.* **10** 1945–53
Fano U and Macek J H 1973 *Rev. Mod. Phys.* **45** 553–73
Flannery M R and McCann K J 1974a *J. Phys. B: At. Mol. Phys.* **7** L223–7
—— 1974b *J. Phys. B: At. Mol. Phys.* **7** 2518–32
—— 1974c *J. Phys. B: At. Mol. Phys.* **7** L522–7
—— 1974d *Phys. Rev.* A **10** 2264–72
—— 1975a *J. Phys. B: At. Mol. Phys.* **8** 1716–33
—— 1975b *Phys. Rev.* A **12** 846–55
Gradshteyn I S and Ryzhik I M 1965 *Tables of Integrals, Series and Products* (New York: Academic) p 672
Hertel I V, Schmidt H, Bähring A and Meyer E 1985 *Rep. Prog. Phys.* **48** 375–414

Johnson L C 1972 *Astrophys. J.* **174** 227–36
Kauppila W E, Ott W R and Fite W L 1970 *Phys. Rev.* A **1** 1099–108
Kingston A E, Fon W C and Burke P G 1976 *J. Phys. B: At. Mol. Phys.* **9** 605–18
Kingston A E, Liew Y C and Burke P G 1982 *J. Phys. B: At. Mol. Phys.* **15** 2755–66
Kingston A E and Walters H R J 1980 *J. Phys. B: At. Mol. Phys.* **13** 4633–62
Long R L, Cox D M and Smith S J 1968 *J. Res. NBS* A **72** 521–35
Macek J and Jaecks D H 1971 *Phys. Rev.* A **4** 2288–300
Madison D H, Hughes J A and McGinness D S 1985 *J. Phys. B: At. Mol. Phys.* **18** 2737–62
Mahan A H, Gallagher A and Smith S J 1976 *Phys. Rev.* A **13** 156–66
Mansky E J 1990a *J. Comput. Phys.* to be submitted
—— 1990b *J. Phys. B: At. Mol. Opt. Phys.* to be submitted
Mansky E J and Flannery M R 1990 *J. Phys. B: At. Mol. Opt. Phys.* **23** L501–7
McCann K J and Flannery M R 1975 *J. Chem. Phys.* **63** 4695–707
—— 1978 *J. Chem. Phys.* **69** 5275–87
McCarthy I E and Stelbovics A T 1983 *J. Phys. B: At. Mol. Phys.* **16** 1611–7
Morgan L A and McDowell M R C 1975 *J. Phys. B: At. Mol. Phys.* **8** 1073–81
Müller-Fiedler R, Schlemmer P, Jung K, Hotop H and Erhardt H 1984 *J. Phys. B: At. Mol. Phys.* **17** 259–68
Scott M P, Scholz T T, Walters H R J and Burke P G 1989 *J. Phys. B: At. Mol. Opt. Phys.* **22** 3055–77
Somerville W B 1963 *Proc. Phys. Soc.* **82** 446–55
Syms R F, McDowell M R C, Morgan L A and Myerscough V P 1975 *J. Phys. B: At. Mol. Phys.* **8** 2817–34
Unnikrishnan K, Prasad M A 1982 *J. Phys. B: At. Mol. Phys.* **15** 1549–57
van Wyngaarden W L and Walters H R J 1985 *J. Phys. B: At. Mol. Phys.* **18** L689–94
—— 1986a *J. Phys. B: At. Mol. Phys.* **19** L53–8
—— 1986b *J. Phys. B: At. Mol. Phys.* **19** 929–68
Vriens L and Smeets A H M 1980 *Phys. Rev.* A **22** 940–51
Whelan C T 1986 *J. Phys. B: At. Mol. Phys.* **19** 2355–63
Whelan C T, McDowell M R C and Edmunds P W 1987 *J. Phys. B: At. Mol. Phys.* **20** 1587–98
Whelan C T and Piraux B 1987 *Phys. Lett.* **122A** 126–8
Williams J F 1975 *J. Phys. B: At. Mol. Phys.* **8** 2191–9
—— 1976 *J. Phys. B: At. Mol. Phys.* **9** 1519–27
—— 1981 *J. Phys. B: At. Mol. Phys.* **14** 1197–217
—— 1986 *Aust. J. Phys.* **39** 621–32
Williams J F and Heck E L 1988 *J. Phys. B: At. Mol. Opt. Phys.* **21** 1627–38
Williams J F and Willis B A 1975 *J. Phys. B: At. Mol. Phys.* **8** 1641–69